Synthesis and Characterization of a Novel Ambipolar Polymer Semiconductor Based on a Fumaronitrile Core as an Electron-Withdrawing Group

Hyung-Gu Jeong,[1] Dongyoon Khim,[1] Eunhwan Jung,[1] Jin-Mun Yun,[1] Juhwan Kim,[1] Jamin Ku,[1] Yun Hee Jang,[1] Dong-Yu Kim[1,2]

[1]School of Materials Science and Engineering, Gwangju Institute of Science and Technology (GIST), 261 Cheomdan-gwagiro, Buk-Gu, Gwangju 500-712, Republic of Korea
[2]School of Nanobio Materials and Electronics, Heeger Center for Advanced Materials (HCAM), GIST, Gwangju 500-712, Republic of Korea
Correspondence to: D.-Y. Kim (E-mail: kimdy@gist.ac.kr)

ABSTRACT: Two conjugated polymers containing stilbene and fumaronitrile moieties were synthesized to investigate their electronic properties by the existence of electron-withdrawing cyano groups on a vinylene backbone. The cyclic voltammetry investigation and time-dependent density functional theory calculations indicated that the cyano substituents lowered the lowest unoccupied molecular orbital (LUMO) energy level by about 0.65 and 0.63 eV, respectively. The lowering of the LUMO energy levels due to the electron-withdrawing properties of the cyano substituents could enhance electron injection capability. Furthermore, bithiophene-fumaronitrile (donor-acceptor) intermolecular interaction facilitates the self-assembly of the polymer chains. Organic field-effect transistors (OFETs) based on PBTSB without the electron-withdrawing group only exhibit hole transport, while OFETs based on PBTFN with cyano substituents exhibit ambipolar characteristics. The growth of PBTFN crystalline fibrils was observed with increasing annealing temperature, which enhanced hole and electron mobility. A complementary-like inverter using PBTFN with ambipolar properties exhibited good symmetry with an inverting voltage nearly half that of the power supply with a gain of 9 at V_{DD} = 100 V. © 2012 Wiley Periodicals, Inc. J. Polym. Sci., Part A: Polym. Chem. **2013**, *51*, 1029–1039

KEYWORDS: ambipolar transport; complementary-like inverter; cyano group; organic field-effect transistor; self-assembly

INTRODUCTION Conjugated polymers are attractive semiconductors for organic field-effect transistors (OFETs),[1,2] organic solar cells (OSCs),[3,4] organic light-emitting diodes (OLEDs),[5,6] and complementary inverter circuits[7,8] because they provide major advantages such as low-cost, large-area, and roll-to-roll manufacturing of organic devices due to simple solution processability.[9,10] Among the various electronic devices, OFETs have been the subject of intensive investigation, and ambipolar transistors are of particular interest because holes and electrons are accumulated simultaneously in both p- and n- channels.[11] For example, complementary circuits require both p- and n- channel operation, but ambipolar semiconductors exhibiting both hole and electron charge transport can be deposited without the need for micropatterning of individual p- and n- channels.[12] In general, ambipolar transistors have been demonstrated using three methods that include a single-layer semiconductor with an intrinsic ambipolar nature, a mixture of p- and n- type semiconductors, and double-layer semiconductor film with hole and electron transport layers.[13,14] Jenekhe and coworkers have reported many promising results from ambipolar transistors using the three methods explained above.[15–17] Among these three methods, to the best of our knowledge the method using a single-layer semiconductor is the best way to fabricate complementary circuits because semiconductor blend and double-layer semiconductor film have problems such as nano-morphology formation in the blend film and intermixing of the bilayers.[17,18]

Electron-withdrawing groups lower the highest occupied molecular orbital (HOMO) and the lowest unoccupied molecular orbital (LUMO) levels; in particular, the lowering of the LUMO energy level is dominated by an electron acceptor.[19] Therefore, the electron can be easily injected from the source-drain electrode into the organic layer due to a low-lying LUMO energy level that is suitable for electron injection and additionally organic materials can have increased oxidative stability due to a low HOMO energy level.[20–22] Here, the energy level of ambipolar semiconductors should be

considered with the work function of the common electrode for ensuring efficient electron injection into the LUMO and hole injection into the HOMO, particularly in the case of a complementary circuit that has a common electrode to minimize the complex micropatterning process. Recently, many low band-gap polymers with alternating donor-acceptor groups have exhibited good ambipolar characteristics.[15,23–25] One of the properties that these polymers have in common is that they have high-lying HOMO energy levels (5.1–5.5 eV) and low-lying LUMO energy levels (3.6–3.9 eV). In addition, the hole-electron balance in the semiconductor films is important for application to complementary circuits. Therefore, it should be noted here that an adequate electron-withdrawing group should be introduced to achieve good balance between hole and electron transport.

Typically, electron-withdrawing groups such as cyano, nitro, and fluoroalkyl are introduced to a p-type conjugated backbone to synthesize n-type organic semiconductors.[26] Vinylene derivatives containing cyano substituents have been studied extensively for organic electronics such as OLEDs, OFETs, and OSCs.[27–34] Particularly, fumaronitrile containing two cyano groups on the vinylic double bond could increase electron injection due to a large electron-withdrawing ability.[20] Recently, Katz and coworkers have demonstrated OFETs based on small molecules containing fumaronitrile moieties and reported the n-type characteristics.[31] To the best of our knowledge, however, ambipolar characteristics of a semiconductor using a fumaronitrile group have not been reported. Therefore, we attempted to synthesize an ambipolar charge-transport semiconducting polymer containing both the thiophene (hole-transporting) moiety and the fumaronitrile (electron-transporting) moiety to demonstrate ambipolar transistors with common source/drain electrodes.

It is difficult to produce a balance between hole and electron mobility when the HOMO energy level is aligned to the work function of the common Au electrode. Therefore, first, the stilbene moiety, containing benzene derivatives instead of thiophene, was introduced, which lowered the HOMO energy level by adjusting the band gap. In addition, the vinylene unit in the stilbene moiety increased the degree of coplanarity. For example, PETV12T containing a thienylenevinylene moiety, recently reported by our group, exhibited a high hole-mobility of 0.15 cm^2 V^{-1} s^{-1} due to the coplanarity of the vinylene unit and the interdigitated structure of PETV12T.[35] Second, two cyano electron-withdrawing groups were introduced to the vinylene unit (fumaronitrile) to lower the LUMO energy level because an elevated LUMO energy level makes electron transport difficult without a buffer layer to improve electron injection. The electronic and structural features (e.g., HOMO/LUMO energy levels, crystallinity, morphology, and charge carrier mobilities) are affected by the nature of the cyano substituents introduced on the conjugated backbone.

In this regard, we first report a fumaronitrile containing ambipolar semiconductor polymer (poly[4,4′-bis(dodecyl)-2,2′-bithiophene-co-bis(phenyl)fumaronitrile] **PBTFN**) via the synthetic strategies for tuning the energy levels. For comparison, a reference semiconductor polymer (poly[4,4′-bis(dodecyl)-2,2′-bithiophene-co-stilbene] **PBTSB**), which does not contain cyano substituents, was synthesized to characterize and compare the effects of cyano substituents. We also demonstrated OFETs and complementary-like inverters based on new synthesized polymers (**PBTSB** and **PBTFN**) to investigate electronic properties by alteration of the backbone structure and introduction of electron withdrawing groups. Furthermore, the molecular geometries and electronic structures of the two synthesized polymers (repeating units of **PBTSB** and **PBTFN**) were investigated by density functional theory (DFT) quantum mechanics calculations.

EXPERIMENTAL

Measurements

^{1}H NMR spectra were measured using a JEOL ECX-400P at 400 MHz. Mass data were obtained using a gas chromatography spectrometry (GCMS) (Shimadzu, GCMS-QP2010). M_n and M_w/M_n of the polymers were measured at 35 °C by gel permeation chromatography, on a system equipped with a guard column (Shodex LF-G), two linear columns (Shodex LF-804), a Model 501 pump (Analytical Scientific Instruments), and an RI-2000 refractive index detector (Schambeck SFD GmbH) using chloroform at 1 mL/min as an eluent. Linear polystyrene standards (Shodex SM-105) were applied for the calibration. Thermal properties of the polymers were determined by DSC (TA Instruments, DSC-Q20) and TGA (TA Instruments, TGA-Q50) at a heating rate of 10 °C/min under a nitrogen atmosphere. The UV–vis spectra of the polymers were measured by using a UV–vis spectrometer (PerkinElmer, lambda 750). Cyclic voltammetry (CV) was conducted using an Autolab PGSTAT 30 potentiostat/galvanostat in an acetonitrile solution with 0.1 M tetrabutylammonium perchlorate as the supporting electrolyte, ITO as the working electrode, a Pt wire as the counter electrode, and Ag wire as the reference electrode at a scan rate of 100 mV s^{-1}. Atomic force microscopy (AFM) images were obtained using a Digital Instruments Multimode AFM controlled by a Nanoscope IIIa scanning probe micro controller. The POM images were all taken on an optical microscope (Olympus BX51) equipped with temperature controlled stages (Linkam LTS 350) and temperature controller (Linkam TMS 94). X-ray diffraction (XRD) was measured using a Rigaku RINT 2000 diffractometer using Cu Kα radiation.

5,5′-Bis(trimethylstannyl)-4,4′-bis(dodecyl)-2,2′-bithiophene (1)

5,5′-Dibromo-4,4′-bis(dodecyl)-2,2′-bithiophene was prepared according to the procedures in the literature.[36] In a two-neck bottom flask, 5,5′-dibromo-4,4′-bis(dodecyl)-2,2′-bithiophene (0.25 g, 0.38 mmol) was dissolved in dry hexane (15 mL) and then cooled to 0 °C. A solution of n-BuLi in cyclohexane (0.57 mL, 1.14 mmol) was added dropwise to a solution of 5,5′-dibromo-4,4′-bis(dodecyl)-2,2′-bithiophene. The reaction mixture was gradually warmed to room temperature and then the mixture was vigorously stirred at 60 °C for 1 h. The reaction mixture was cooled to −0 °C and then trimethyltin chloride (1.20 mL; 1.20 mmol) was added

dropwise to the reaction mixture, which was then let stand overnight at room temperature. The resultant mixture was extracted with methylene chloride and washed with distilled water and brine. The combined organic fractions were dried over anhydrous $MgSO_4$, and then filtered under reduced pressure to give the product. The crude product was followed by purification using column chromatography with hexanes as an eluent, which provided the analytical pure product (0.28 g) in an 89% yield. ^1H NMR (400 MHz; $CDCl_3$; Me_4Si): δ (ppm) 7.10 (s, 2H), 2.54 (t, J = 7.8 Hz, 4H), 1.58 (m, 4H), 1.26 (m, 36H), 0.88 (m, 6H), 0.37 (m, 18H); ^{13}C NMR (100 MHz; $CDCl_3$; ppm): δ = 151.48, 142.68, 130.78, 125.83, 32.86, 32.00, 31.92, 29.84, 29.79, 29.66, 29.64, 29.63, 29.61, 29.58, 22.71, 14.09, −7.89; (Note: 29.84–29.58 peaks in the ^{13}C NMR spectrum overlap).

Bis(4-bromophenyl)fumaronitrile (2)

A two-neck flask was charged with 4-bromophenylacetonitrile (2.00 g, 10.2 mmol) and iodine (2.59 g, 10.2 mmol) in dry ether (50 mL) and cooled to −78 °C. A solution of sodium methoxide (1.38 g, 25.5 mmol) in methanol (10 mL) was added into the reaction solution at −78 °C under a nitrogen atmosphere. The reaction mixture was gradually warmed to 0 °C and then the mixture was stirred at 0 °C for 4 h. The reaction was quenched with a 3% aqueous solution of hydrochloric acid. The solution was filtered to isolate the solid, which was rinsed with methanol to remove the ionic residues. Finally, the remaining white solid was dried under vacuum and the product was recrystallized from methylene chloride as a white solid (1.45 g) in a 72% yield. ^1H NMR (400 MHz; $CDCl_3$; Me_4Si): δ (ppm) 7.71–7.65 (m, 8H); ^{13}C NMR (100 MHz; $CDCl_3$; ppm): δ = 132.7, 130.5, 130.1, 126.8, 124.6, 116.1; MS (EI): m/z = 387.90 $[M]^+$ (Calcd: 387.85).

Trans-4,4′-dibromostilbene (3)

A two-neck flask was charged with zinc powder (6.31 g, 96.6 mmol) in anhydrous THF (100 mL), and $TiCl_4$ (9.16 g, 48.3 mmol) was added dropwise to the solution at 0 °C. Then, a solution of 4-bromobenzaldehyde (3 g, 16.2 mmol) in anhydrous THF (50 mL) was added into the reaction solution at 0 °C. The reaction mixture was vigorously stirred at 70 °C for 5 h. After 5 h, the reaction mixture was poured into a separating funnel with aqueous $NaHCO_3$ solution, and then the aqueous layer was extracted with methylene chloride while the combined organic layer was dried over anhydrous $MgSO_4$ and concentrated under reduced pressure to give the crude product. Finally, the crude product was recrystallized from methylene chloride as a white solid (2.35 g) in an 86% yield. ^1H NMR (400 MHz; $CDCl_3$; Me_4Si): δ (ppm) 7.49 (d, J = 8.7 Hz, 4H), 7.37 (d, J = 8.5 Hz, 4H), 7.02 (s, 2H); ^{13}C NMR (100 MHz; $CDCl_3$; ppm): δ = 135.9, 131.9, 128.1, 128.0, 121.6; MS (EI): m/z = 338.04 $[M]^+$ (Calcd: 337.65).

Poly[4,4′-bis(dodecyl)-2,2′-bithiophene-co-bis(phenyl)fumaronitrile] (PBTFN)

In a 50 mL, flame-dried, two-neck flask, Compound **1** (0.300 g, 0.362 mmol), Compound **2** (0.140 g, 0.361 mmol), P(o-tolyl)$_3$ (0.003 g, 0.010 mmol), and Pd_2dba_3 (0.007 g, 0.008

mmol) was dissolved in dry chlorobenzene (10 mL). The reaction mixture was stirred at 120 °C for 48 h under N_2. Bromobenzene (0.28 g, 1.75 mmol) was added, and stirred for 2 h, followed by the addition of 2-(tributylstannyl) thiophene (0.65 g, 1.75 mmol), and the reaction mixture was stirred for 2 h. After cooling to room temperature, the resultant mixture was precipitated into a mixture of methanol (90 mL) and concentrated hydrochloric acid (10 mL) with stirring for 1 h at room temperature. The precipitate was filtered and washed several times with methanol. The unreacted monomers and low-molecular-weight fractions were removed by Soxhlet extraction with methanol, and hexane. The soluble fraction was collected by extraction with chloroform. Yield: 0.124 g (47%); ^1H NMR (400 MHz; $CDCl_3$; Me_4Si): δ (ppm) 7.94–7.45 (m, br, 8H) 7.14 (br, 2H), 2.71 (br, 4H), 1.68 (br, 4H) 1.26 (br, 36H), 0.87 (br, 6H).

Poly[4,4′-bis(dodecyl)-2,2′-bithiophene-co-stilbene] (PBTSB)

The same procedure as described for **PBTFN** was followed. Compound **1** (0.350 g, 0.422 mmol), Compound **3** (0.140 g, 0.414 mmol), P(o-tolyl)$_3$ (0.005 g, 0.016 mmol), and Pd_2dba_3 (0.009 g, 0.010 mmol) was dissolved in dry chlorobenzene. Yield: 0.085 g (31%); ^1H NMR (400 MHz; $CDCl_3$; Me_4Si): δ (ppm) 7.59 (br, 4H) 7.48 (br, 4H), 7.08 (br, 2H), 7.00 (br, 2H) 2.67 (br, 4H), 1.65 (br, 4H) 1.26 (br, 36H), and 0.87 (br, 6H).

OFET Device Fabrication and Characterization

OFETs were fabricated in a TG/BC configuration on a glass substrate. The fabricated FETs had a channel length of 20 μm and a channel width of 1.0 mm. The source/drain electrodes were patterned using photolithography and then were deposited by thermal evaporation of 3 nm of Ni and 12 nm of Au. For FET fabrication, the substrates were ultrasonicated in acetone and again in isopropanol. The substrates were exposed to UV/O_3 treatment in air for 20 min. After the thin films of the organic semiconductors were spin coated (2000 rpm, 60 s) from a solution of **PBTSB** and **PBTFN** (10 mg/mL, chlorobenzene), substrates were annealed at 100, 150, 200, and 250 °C for 20 min, then thin films of CYTOP:CT-sol.180 (2:1 blend, thickness 500 nm, Asahi Glass) were spin coated at 2,000 rpm for 60 s. The devices were completed by deposition of a 50 nm Al layer by thermal evaporation. The current–voltage (I–V) characteristics of the OFET devices were measured using a Keithley 4200-SCS under N_2 inert conditions.

Complementary Inverter Fabrication

The contact electrodes (Au/Ni) of the inverters were patterned by applying the same method as described above and consisted of individual FET electrodes [$L_{p,n}$ = 20 μm, W_p = 1 mm, W_n = 10 mm]. The thin film of **PBTFN** was prepared by spin-coating and annealed at 200 °C for 20 min. The rest of the procedure is the same as described above.

RESULTS AND DISCUSSION

General Synthesis

The synthetic procedures are illustrated in Scheme 1. The bis(4-bromophenyl)fumaronitrile was prepared from
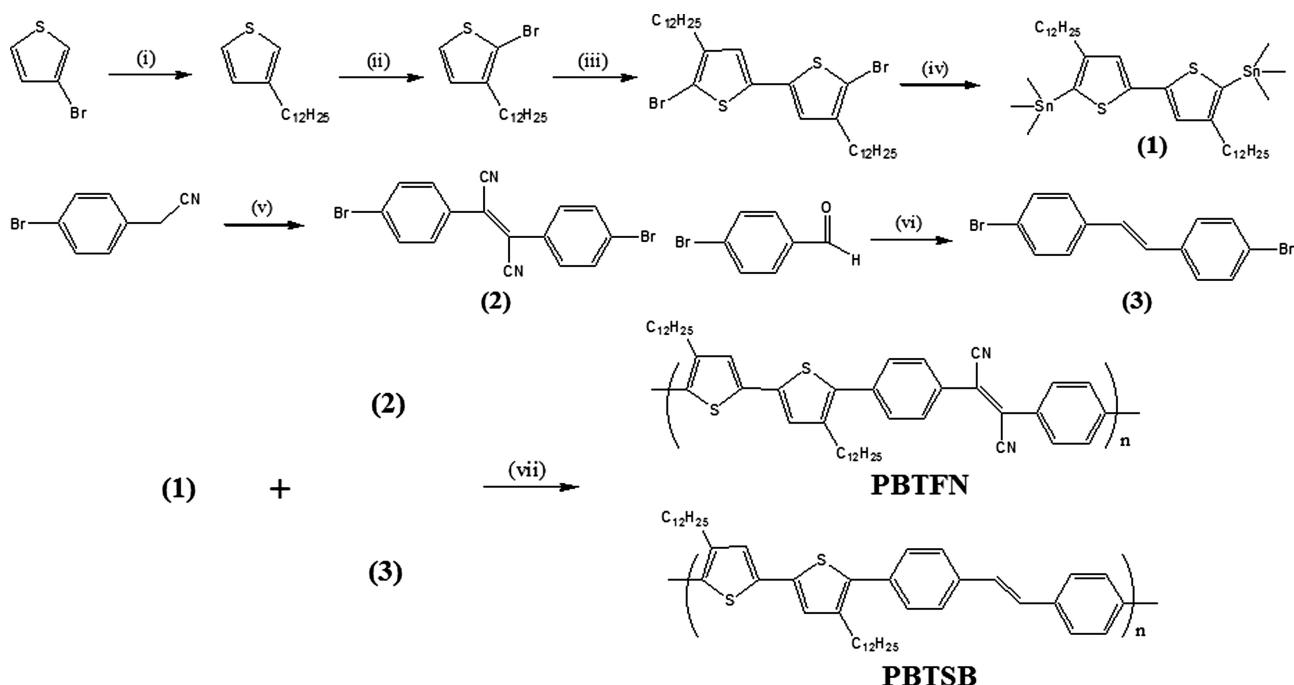
SCHEME 1 Synthesis of **PBTSB** and **PBTFN**. (i) $C_{12}H_{25}MgBr$, Ni(dppp)Cl$_2$, diethyl ether, 50 °C. (ii) NBS, AcOH, chloroform, rt. (iii) AgNO$_3$, KF, PdCl$_2$(PhCN)$_2$, DMSO, 70 °C . (iv) n-BuLi, trimethyltin chloride, hexane, 0 °C. (v) I$_2$, Na$_2$OCH$_3$, MeOH, diethyl ether, −78 °C. (vi) Zn, TiCl$_4$, THF, 0 °C. (vii) Pd$_2$(dba)$_3$, P(o-tolyl)$_3$, chlorobenzene, reflux.

4-bromophenylacetonitrile, iodine, and sodium methoxide in dry diethyl ether. When two equivalents of sodium methoxide, a critical component of this reaction, were added in reaction mixtures, the formation of a (Z)-isomer could be minimized.[37] The purity was checked after twice recrystallizations by measuring the proton NMR spectra. It was confirmed that 4,4′-dibromostilbene and bis(4-bromophenyl)fumaronitrile did not contain a (Z)-isomer. The polymerization was performed by Stille cross-coupling, and low molecular-weight fractions were removed by Soxhlet extraction with methanol, and hexane. The soluble fraction was collected by extraction with chloroform, and then the polymer powders were obtained by reprecipitation in methanol. The M_n of **PBTSB** and **PBTFN** were 6,500 and 9,500 Da, respectively, and the polydispersity index (PDI) (M_w/M_n) of **PBTSB** and **PBTFN** were 1.15 and 1.65, respectively. The M_n was determined by polystyrene standards in chloroform. The polymers were highly soluble in common organic solvents such as THF, chloroform, and chlorobenzene, and the spin-coated films had good uniformity.

Optical Properties of PBTSB and PBTFN

The absorption spectra of **PBTSB** and **PBTFN** obtained in solution and film states are shown in Figure 1, and the characterization of **PBTSB** and **PBTFN** are summarized in Table 1. The absorption maxima of **PBTFN** in the film and solution states were significantly red-shifted compared with those of **PBTSB**. In fact, the chemical structure of **PBTFN** was similar to that of **PBTSB** except that it contained cyano groups. These results demonstrate that the cyano group acts as an electron-withdrawing group, and the absorption bands at

470 and 495 nm in **PBTFN** correspond to the electronic state of an electron acceptor and a charge-transfer character by the electron-withdrawing group. The band-gap of **PBTFN** was decreased by 0.38 eV after introduction of the cyano group compared to that of **PBTSB**, and this was attributed to an intramolecular charge transfer (ICT) interaction between the bis(dodecyl)bithiophene (electron donor, D) and bis(phenyl)fumaronitrile (electron acceptor, A) moieties along the polymer chain. In addition, **PBTFN** exhibited two absorption bands, unlike the single characteristic absorption band of **PBTSB**, and the spectral band around 350 nm was assigned to the π→π* transition for **PBTFN**. The two characteristic absorption bands of the **PBTFN** thin films were quite
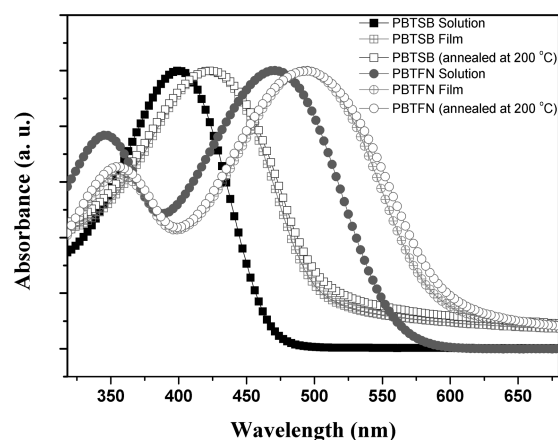
FIGURE 1 UV–vis spectra of **PBTSB** and **PBTFN** in chlorobenzene, film, and annealed film states.

TABLE 1 A Summary of the Characterization of **PBTSB** and **PBTFN**

Polymer	M_n^a (kDa)	PDI^a	T_d^b (°C)	Absorbance λ_{max} [solution^c, film^d (nm)]	E_g (optical)^e (eV)	E_{HOMO}^f (eV)	E_{LUMO}^g (eV)
PBTSB	6.5	1.15	395	400, 422	2.48 (2.94)	5.38	2.90 (3.22)
PBTFN	9.5	1.65	396	470, 495	2.10 (2.51)	5.65	3.55 (3.53)

^{a} M_n and PDI determined by polystyrene standards in chloroform.
^{b} T_d (5% weight loss) determined by TGA under N_2.
^{c} Measured in chlorobenzene.
^{d} Cast from chlorobenzene.
^{e} Energy bandgap estimated from the onset wavelength (or from the absorbance maximum λ_{max}) of the optical absorption in film states.
^{f} HOMO = $[E_{ox}^{onset} - E_{1/2(ferrocene)}] + 4.8$ eV.
^{g} The LUMO energy level estimated from optical band gap (or from the onset potential of reduction wave).

similar in shape to those in the solution state. A maximum absorption peak at 357 nm derived from the $\pi \rightarrow \pi^*$ transition for **PBTFN** thin film was red-shifted 11 nm compared with the corresponding peak in the solution state. Another maximum absorption peak corresponding to the ICT was red-shifted 25 nm in the film state. In general, the molecular chain had a much more planar conformation by the formation of a π-stacked structure in the solid state, resulting in an increased electronic delocalization length, so that maximum absorption moved to longer wavelengths. However, maximum absorption peaks corresponding to the $\pi \rightarrow \pi^*$ transition and ICT were slightly red-shifted in going from the solution to the solid state. This small red-shift could be attributed to the planar and rigid properties of vinylene moieties in the solution state; in other words, there was no significant conformational difference between the solution and the solid state. Meanwhile, the broad absorption bands of **PBTSB** and **PBTFN** in the solid state suggested π-π stacking in the polymer film. The absorption spectra of thermally annealed **PBTFN** and **PBTSB** film exhibited broad absorption compared with that of non-annealed film. Otherwise, there were no significant differences, regardless of the morphological changes.

Thermal Properties

Thermal properties of **PBTSB** and **PBTFN** were investigated using thermogravimetric analysis (TGA) and differential scanning calorimetry (DSC). The degradation temperatures (T_d) at 5% weight loss of **PBTSB** and **PBTFN** were detected at 395 and 396 °C, respectively, which demonstrates that these polymers possess good thermal stability [Fig. 2(a)]. From the DSC measurements [Fig. 2(b)], **PBTSB** exhibited no transition peak including T_g and T_m during the heating and cooling scans. However, **PBTFN** revealed an obvious exothermic transition at 163 and 185 °C during the cooling scan and a weak endothermic transition at 190 and 210 °C during the second heating scan. The exothermic (at 163 and 185 °C) and endothermic (at 190 and 210 °C) transitions correspond, respectively, to the recrystallization and crystal melting peaks. The two endothermic transitions at 190 and 210 °C on the second heating scan of **PBTFN** may correspond to crystal-to-liquid crystal and liquid crystal-to-isotropic phase transitions.[35] The reason why only **PBTFN** showed the obvious transition peaks is that the electron-de-

ficient CN unit provided an additional intermolecular interaction with the electron-rich thiophene unit.[26]

Electrochemical Properties

CV was performed to understand the electrochemical characteristics of the **PBTSB** and **PBTFN** using 0.1 M Bu_4NClO_4 in acetonitrile as an electrolyte at a scan rate of 100 mV s^{-1}. To investigate the electrochemical properties of the polymers, a thin film was prepared on indium tin oxide glass as a working electrode, and silver and platinum wires
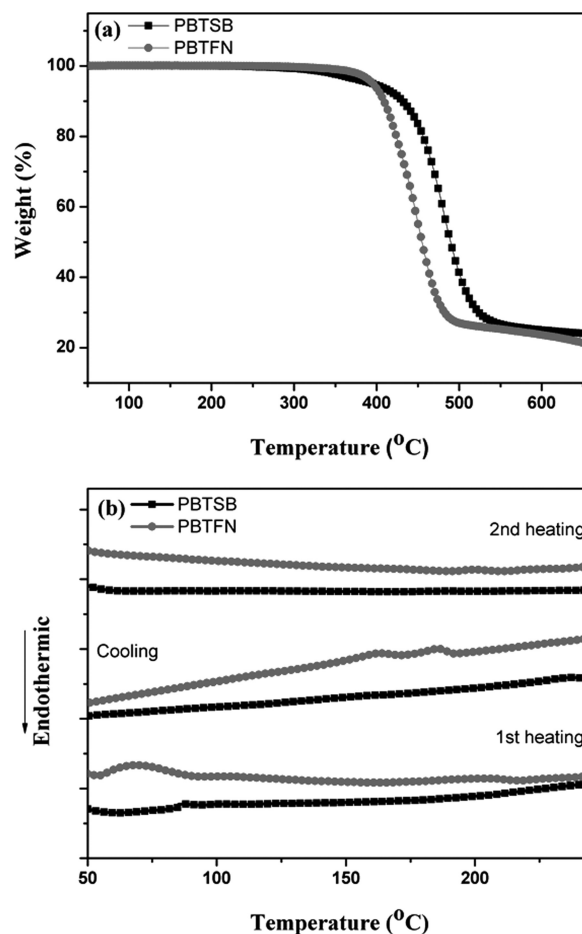
FIGURE 2 TGA (a) DSC (b) curves of **PBTSB** and **PBTFN** with a heating and cooling rate of 10 °C min^{-1} under N_2 atmosphere.
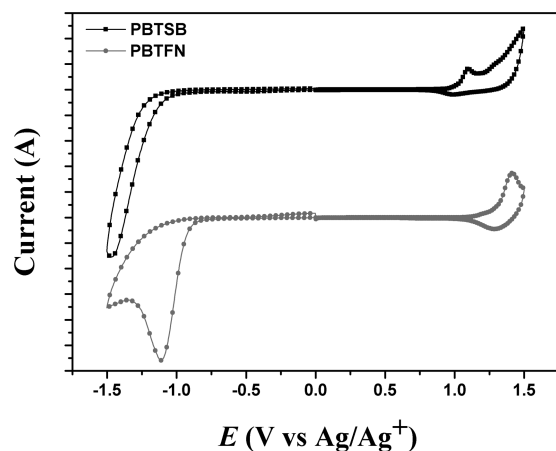
FIGURE 3 Cyclic voltammogram of **PBTSB** and **PBTFN** in 0.1 M Bu₄NClO₄, acetonitrile solution at a scan rate of 100 mV s⁻¹.

FIGURE 4 Energy level diagrams of **PBTSB** and **PBTFN** (TDDFT calculations and CV).

were used as the reference and counter electrodes, respectively. As shown in Figure 3, the onset oxidation potentials for **PBTSB** and **PBTFN** versus Ag/Ag⁺ were found to be +1.01 and +1.28 V, respectively. The HOMO energy level was calculated with reference to the half-wave potential of ferrocene/ferrocenium (Fc/Fc⁺), 4.8 eV below the vacuum level, according to the following equation: HOMO = $-[E_{ox}^{onset} - E_{1/2(ferrocene)}] - 4.8$ eV.[38] The LUMO energy level was calculated from the estimated optical band gap (not the onset potential of reduction wave) because the E_g (TDDFT) was calculated using optical absorption data. The

corresponding HOMO energy levels of **PBTSB** and **PBTFN** were −5.38 and −5.65 eV, and the LUMO energy levels were −2.90 and −3.55 eV, respectively. The introduction of a stilbene unit instead of bis(thienyl)ethylene lowered the HOMO energy level and elevated the LUMO energy level due to the large band gaps of the phenylene derivatives.[39] The HOMO and LUMO energy levels of **PBTFN** were, 0.27 and 0.65 eV, respectively, lower than those of **PBTSB** due to the introduction of an electron withdrawing cyano group
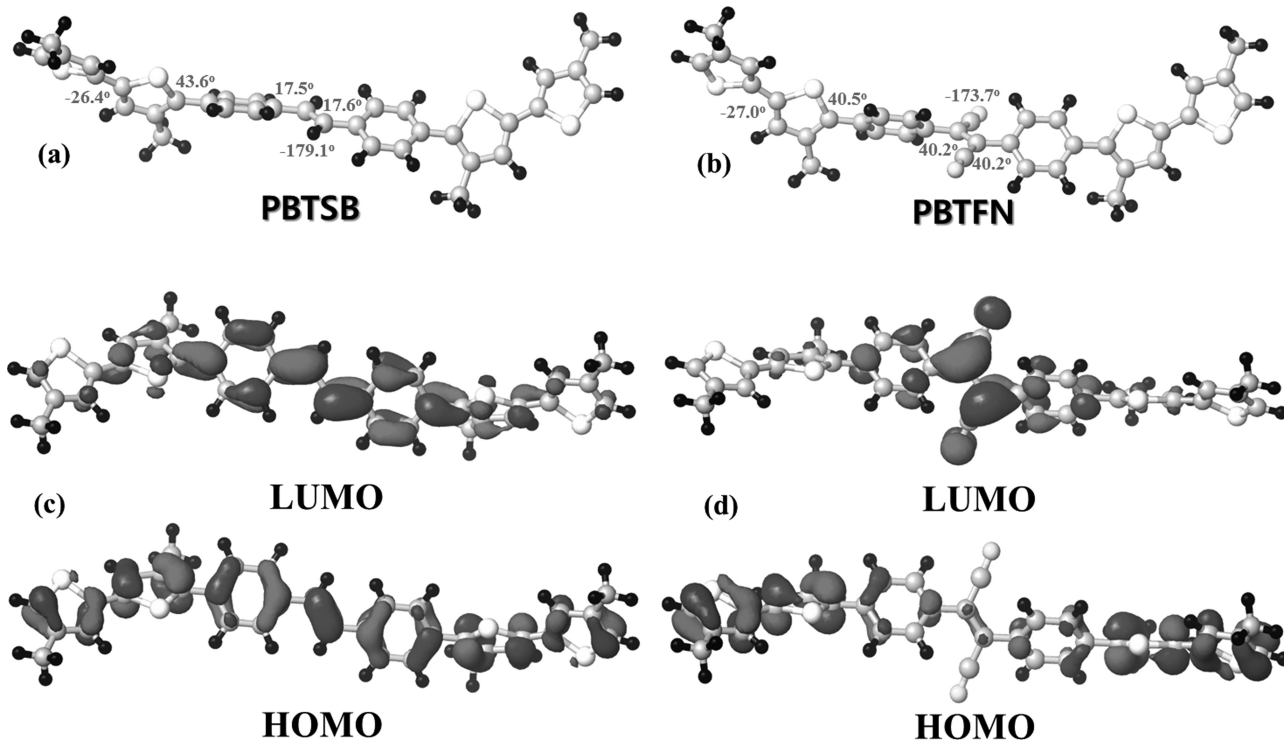
FIGURE 5 Optimized molecular structures of **PBTSB** and **PBTFN** (a, b) and their molecular orbital (MO) diagrams (c,d). Several torsion angles are shown together in red bold faces. Color code: black (H), gray (C), green (N), yellow (S), red, and blue (positive and negative phases of MO).
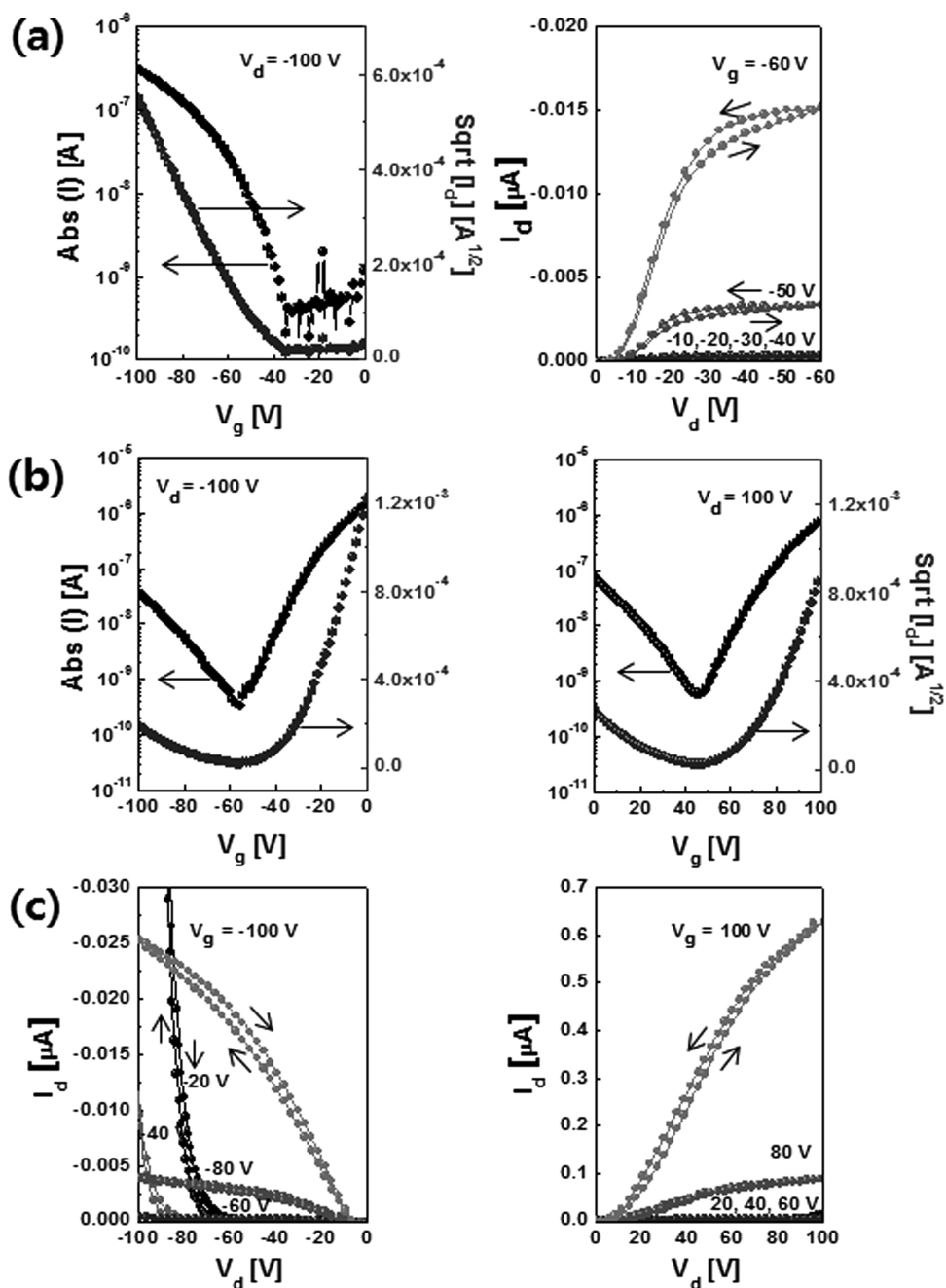
FIGURE 6 I–V characteristics of an OFET device with **PBTSB** and **PBTFN** as the semiconductor: Transfer and output curves of **PBTSB** (a); transfer (b) and output (c) curves of ambipolar **PBTFN**.

as we originally intended. In particular, the large differences (0.65 eV) of the LUMO energy levels between **PBTFN** and **PBTSB** were attributed to the large variation in LUMO energy levels of **PBTFN** due to the strong electron-withdrawing group (fumaronitrile) and to the effect of lowering the HOMO-LUMO energy gap by the push-pull structure. HOMO and LUMO energy levels of **PBTFN** were significantly lower than those of the P3HT, which is well known as a typical p-type material. Taking these facts into consideration, **PBTFN** could reduce the electron injection barrier.

Molecular Geometry and Electronic Structure

It is well known that the carrier mobility of organic semiconductors depends significantly on molecular geometry (planarity) and electronic structure. The influences of the two cyano groups on the geometry and on the electronic structure were investigated with DFT calculations. The geometries of repeating-unit models of **PBTSB** and **PBTFN** were optimized in the gas phase at the level of B3LYP/6-311G(d,p) using the *Jaguar* v6.5 software.[40,41] As shown in Figure 5(a,b), both **PBTSB** and **PBTFN** show significant twists (43.6° and 40.5°, respectively) between thiophenes and

adjacent benzene rings, most likely due to the steric hindrance between the dodecyl (methyl in our models) side chains and the benzene rings. A prominent influence of the two cyano groups introduced to the vinylene moiety is a large twisting of the bis(phenyl)fumaronitrile backbone (from $17.5°$ of rather planar **PBTSB** to $40.2°$ of nonplanar **PBTFN**).

Such change in the molecular geometry explains (or originates from) the difference in the electronic structure between the two polymers. Figure 5(c,d) shows the frontier molecular orbitals (HOMO and LUMO) of each polymer model, which are superimposed on top of the optimized structure. In the case of **PBTSB** [Fig. 5(c)], both HOMO and LUMO are well distributed over the whole backbone, except a slight localization of the LUMO around the stilbene moiety. A rather extended π-conjugation and in turn a certain degree of planarity is expected for **PBTSB**. However, after the introduction of the cyano substituents, **PBTFN** [Fig. 5(d)] exhibits rather localized HOMO (on the thiophene "donor" moieties) and LUMO (on the fumaronitrile "acceptor" moieties). This explains the prominent twisting of the backbone around the fumaronitrile.

The MO energy levels (E_{HOMO} and E_{LUMO}) were taken from the DFT eigenvalue (E_{HOMO}; -5.28 and -5.62 eV for **PBTSB** and **PBTFN**, respectively) and from the lowest electronic transition energy (band gap; E_g; 2.94 and 2.51 eV) calculated with a TDDFT method implemented in the Gaussian 03 program [$E_{LUMO} = E_{HOMO}$ (DFT) $+ E_g$ (TDDFT); -2.39 and -3.35 eV].[42] As shown in Figure 4, the calculated values are in reasonable agreement with the experimental values obtained from the CV (E_{HOMO}) and the absorbance maximum wavelength (E_g). They again indicate that the two cyano electron-withdrawing groups led to the low-lying HOMO and LUMO of **PBTFN**. The lowering is more significant for fumaronitrile-centered LUMO than for thiophene-centered HOMO, leading to the reduced band gap of **PBTFN**.

Characterization of the FET Devices and Complementary Circuits

The charge-carrier mobility of the new polymers was measured using field-effect transistors (FETs) with top-gate/bottom-contact (TG/BC) geometry, which were set up as described in the experimental section. Although these newly synthesized polymers (**PBTSB** and **PBTFN**) have a very similar chemical structure, electron injection could be enhanced by the introduction of a cyano group into the stilbene moiety. The n-type characteristics of transistors based on fumaronitrile containing two cyano groups have not yet been reported without surface treatments for efficient electron injection. The transistors based on **PBTSB** typically exhibited p-type characteristics, as shown in Figure 6. The low mobility of **PBTSB** might be due to the large dihedral angle of phenyl rings, which increases conformational disorder. Indeed, a phase transition peak was not detected by DSC measurements, and evidence of crystallinity was not confirmed by XRD analysis. Considering these results, **PBTSB** was amorphous as expected. However, the transistor based

TABLE 2 Summary of OFETs Mobilities for **PBTSB** and **PBTFN** at Various Temperatures

Polymers	$T_{annealing}$ (°C)	μ_h[a] (cm^2 V^{-1} s^{-1})	μ_e[a] (cm^2 V^{-1} s^{-1})
PBTSB	100	8.5×10^{-4}	–
	150	5.5×10^{-4}	–
	200	8.7×10^{-4}	–
	250	8.9×10^{-4}	–
PBTFN	100	1.2×10^{-5}	8.1×10^{-4}
	150	1.0×10^{-4}	1.2×10^{-3}
	200	1.4×10^{-4}	3.0×10^{-3}
	250	5.4×10^{-5}	1.4×10^{-3}

[a] Mobilities were calculated using equation $I_D = (\mu WC/2L)(V_g - V_t)^2$. C, capacitance; L, length; W, width.

on **PBTFN** exhibited ambipolar charge transport characteristics due to the introduction of an electron-withdrawing cyano group; moreover, electron mobility was higher than hole mobility. These ambipolar characteristics have never been observed in organic semiconductors using the fumaronitrile moiety.

To obtain high carrier mobilities, it is important to arrange the polymer molecules in a specific molecular direction for preferable charge transport in the OFET architecture. Therefore, thermal annealing usually improves mobility compared with nonannealed devices due to enhanced intermolecular ordering and π-π stacking. Thermal annealing effects such as enhancement of charge-carrier mobility usually take place when the polymers of the semiconducting layer have an ordered phase after annealing.[43] The FET characteristics of **PBTSB** and **PBTFN** at different annealing temperature are summarized in Table 2. It can be inferred that **PBTSB** was insensitive to thermal treatment and did not form an ordered phase because there was no relative variation of mobility in the transistor based on **PBTSB** after annealing. However, the hole and electron mobilities of the transistor based on **PBTFN** increased with increasing annealing temperature up to 200 °C but decreased at an annealing temperature of 250 °C. We observed the morphological changes of **PBTSB** and **PBTFN** films with temperature variation using AFM to investigate the relationship between annealing temperature and charge-carrier mobility. Figure 7 shows the AFM phase images of annealed **PBTFN** film at different annealing temperatures. Interestingly, the **PBTSB** film showed a slightly aggregated morphology at higher temperature, but otherwise there were no distinguishable morphological changes. However, **PBTFN** film began to show a fibrillar structure after annealing at 150 °C, and mature fibrils were observed in **PBTFN** film annealed at 200 °C. The fibrillar structure disappeared, and a rough surface was observed due to aggregation in **PBTFN** film annealed at 250 °C. This clearly showed that the annealing temperature dependence of the mobility is related to the morphology of **PBTFN** film. We also observed polarized optical microscopy (POM) images to confirm the presence of the crystalline phase because of the observation of a fibrillar structure. Crystalline
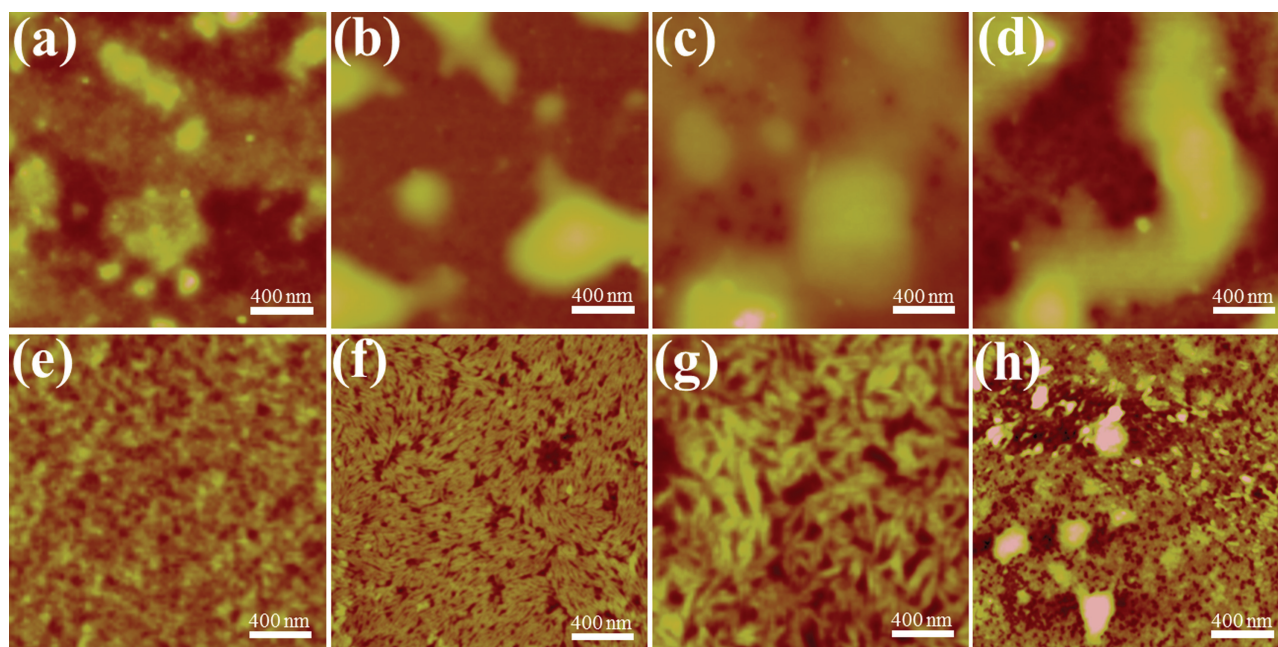
FIGURE 7 AFM topographic images of spin-coated **PBTSB** (a–d) and **PBTFN** (e–h) films on SiO$_2$/Si substrate at different annealing temperature for 20 min; (a, e): 100 °C, (b, f): 150 °C, (c, g): 200 °C, (d, h): 250 °C.

PBTSB was not observed as we intended, but **PBTFN** film exhibited crystals after annealing above 150 °C. There was no significant difference between the POM images of films annealed at 150 °C and those annealed at 200 °C. However, similar to the AFM image of **PBTFN**, the POM image exhibited large aggregates of crystals after annealing at 250 °C as shown in Figure 8. The AFM and POM images for various annealing temperature were entirely consistent with the var-iations in charge-carrier mobility in the OFETs based on **PBTSB** and **PBTFN**.

In general, the nonplanar molecular structure prevented close molecular packing, and the localized molecular orbital hindered charge transport.[44] The DFT calculation revealed that the **PBTFN** repeat unit has a twisted molecular structure and localized molecular orbital compared to **PBTSB**. However, OFETs based on **PBTFN** exhibited higher charge-
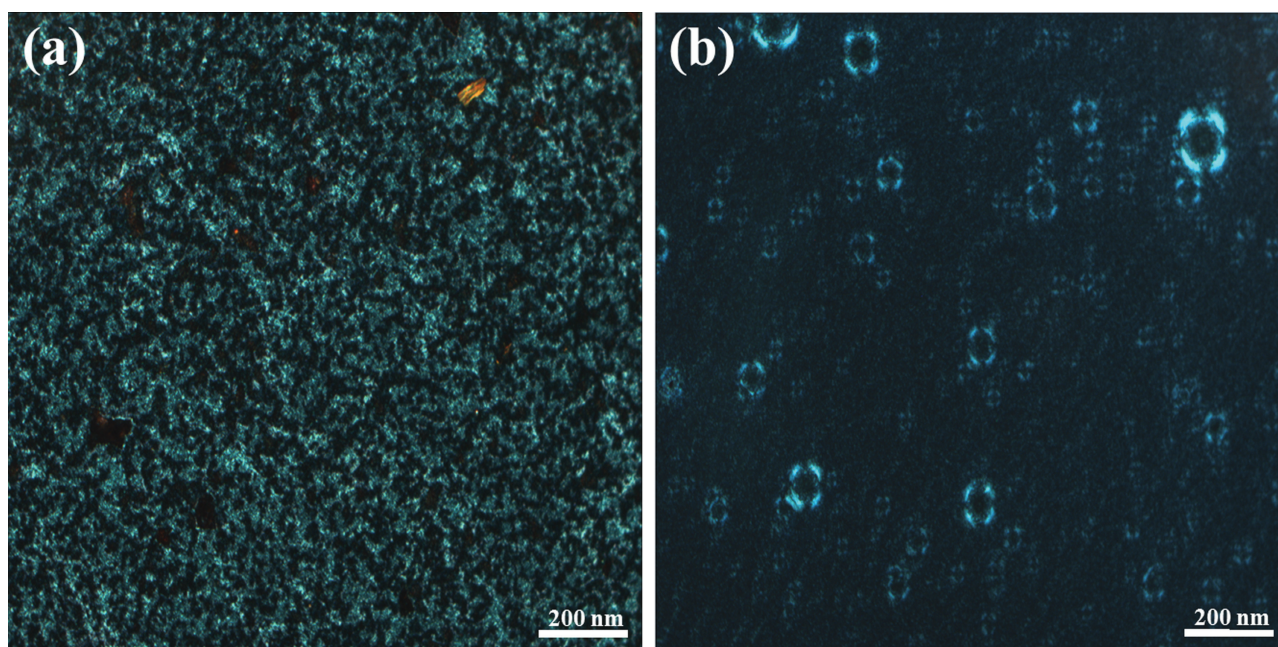
FIGURE 8 POM images of **PBTFN** at different annealing temperature for 20 min: (a) 200 °C and (b) 250 °C.
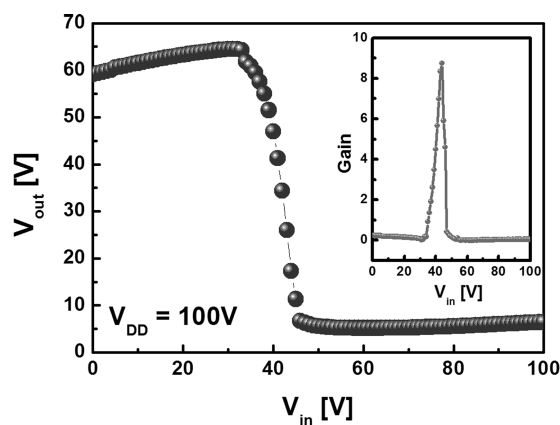
FIGURE 9 VTC of a complementary inverter consisting of an ambipolar **PBTFN** FETs.

carrier mobility after thermal annealing. The fibrillar structure of **PBTFN** may be driven by an electron-withdrawing cyano group that led to the strong intermolecular interactions.[45,46] It is well known that charge transport can be dominated by the hopping mechanism, and intermolecular π-π interactions could reduce disordered regions and insulating grain boundaries.[47] In the case of OFETs based on **PBTFN**, electron transport was improved because of their well-ordered molecular packing in fibrillar structure.[48,49] We demonstrated a complementary-like inverter using two identical ambipolar FETs with a common gate as input voltages and a common drain as output voltages.[13] Figure 9 shows the voltage-transfer characteristics (VTC) of a CMOS-like inverter based on **PBTFN** ($L_{p,n} = 20$ μm, $W_p = 1$ mm, $W_n = 10$ mm). **PBTFN** CMOS inverters showed a Z-shaped VTC curve, which is generally exhibited by CMOS inverters, based on ambipolarity due to the parasitic current of a single transistor.[50] However, the VTC of the inverter exhibited a good symmetry with an inverting voltage nearly half that of the power supply with a gain of 9 at $V_{DD} = 100$ V. Furthermore, we investigated the stability of **PBTSB**- and **PBTFN**-based

transistors. The relative humidity during the period of measurement was maintained at 30–35%. The p-channels of **PBTSB** and **PBTFN** showed relatively stable performance under air-exposed conditions, while the n-channel of **PBTFN** showed poor air-stability, as shown in Figure 10. The low-lying HOMO energy level (E_{HOMO}; -5.38 and -5.65 eV for **PBTSB** and **PBTFN**, respectively) led to stable device performance under ambient conditions compared with the n-channel of **PBTFN**. In addition, the poor stability of the n-channel OFETs was attributed to the presence of electron traps in the air.

CONCLUSIONS

Two conjugated polymers containing stilbene and fumaronitrile moieties were synthesized using a Stille cross-coupling reaction, and OFETs were fabricated using synthesized polymers. We investigated the effects of electron-withdrawing cyano groups on the electronic properties of the new conjugated polymers. **PBTFN** possessed low HOMO and LUMO energy levels compared to those of **PBTSB** due to the electron-withdrawing effects of the cyano groups; in particular, the lowering of the LUMO energy levels was noticeable. **PBTFN** exhibited ambipolar transport behavior, and **PBTSB** as a reference material only exhibited hole transport properties in OFETs because the lower LUMO energy levels of **PBTFN** facilitated electron injection from the electrodes into the semiconductor. Although, based on DFT calculation, **PBTFN** possessed localized electron density along the backbone and a twisted molecular structure, which might interrupt charge transport, however, OFETs based on **PBTFN** exhibited higher mobility compared with those of **PBTSB** due to enhanced intermolecular ordering. Ambipolar transport in OFETs using the polymer containing a fumaronitrile moiety was observed for the first time, and a complementary-like inverter using two identical ambipolar FETs with a common gate and a common drain exhibited a good voltage gain despite relatively low mobility.
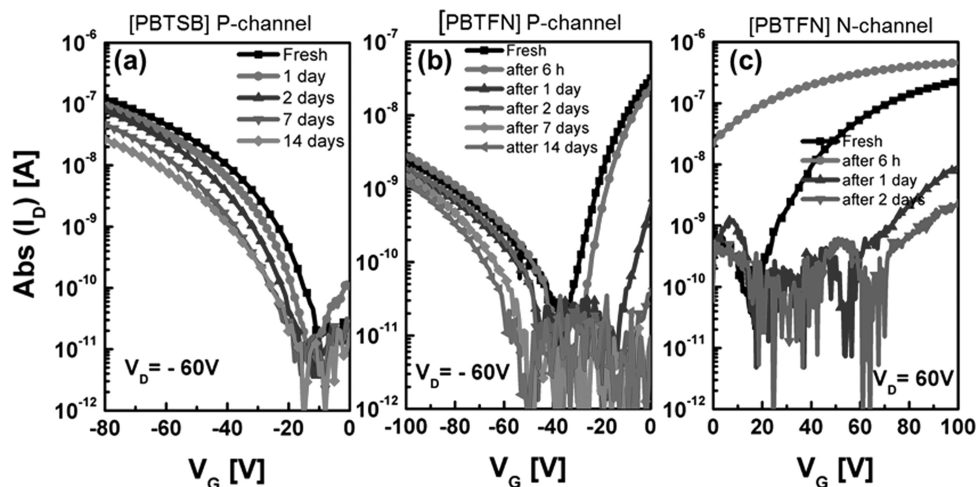
FIGURE 10 Transfer curves of **PBTSB** and **PBTFN** OFETs with different time of exposed to ambient air: p-type of **PBTSB** (a); p-type (b) and n-type (c) of ambipolar **PBTFN**.

REFERENCES AND NOTES

1 H. Usta, G. Lu, A. Facchetti, T. J. Marks, *J. Am. Chem. Soc.* **2006**, *128*, 9034–9035.

2 H. Nakanotani, M. Saito, H. Nakamura, C. Adachi, *Appl. Phys. Lett.* **2009**, *95*, 033308.

3 W. Ma, C. Yang, X. Gong, K. Lee, A. J. Heeger, *Adv. Funct. Mater.* **2005**, *15*, 1617–1622.

4 C. J. Brabec, N. S. Sariciftci, J. C. Hummelen, *Adv. Funct. Mater.* **2001**, *11*, 15–26.

5 D. Vak, C. Chun, C. L. Lee, J.-J. Kim, D.-Y. Kim, *J. Mater. Chem.* **2004**, *14*, 1342–1346.

6 R. Yang, R. Tian, Q. Hou, W. Yang, Y. Cao, *Macromolecules* **2003**, *36*, 7453–7460.

7 Z. Chen, H. Lemke, S. Albert-Seifried, M. Caironi, M. M. Nielsen, M. Heeney, W. Zhang, I. McCulloch, H. Sirringhaus, *Adv. Mater.* **2010**, *22*, 2371–2375.

8 K.-J. Baeg, D. Khim, J.-H. Kim, M. Kang, I.-K. You, D.-Y. Kim, Y.-Y. Noh, *Org. Electron.* **2011**, *12*, 634–640.

9 F. C. Krebs, J. Fyenbob, M. Jørgensen, *J. Mater. Chem.* **2010**, *20*, 8994–9001.

10 J. H. Cho, J. Lee, Y. Xia, B. Kim, Y. He, M. J. Renn, T. P. Lodge, C. D. Frisbie, *Nat. Mater.* **2008**, *7*, 900–906.

11 H. Nakanotani, M. Saito, H. Nakamura, C. Adachi, *Appl. Phys. Lett.* **2009**, *95*, 103307.

12 T. D. Anthopoulos, S. Setayesh, E. Smits, M. Cölle, E. Cantatore, B. de Boer, P. W. M. Blom, D. M. de Leeuw, *Adv. Mater.* **2006**, *18*, 1900–1904.

13 K.-J. Baeg, J. Kim, D. Khim, M. Caironi, D.-Y. Kim, I.-K. You, J. R. Quinn, A. Facchetti, Y.-Y. Noh, *ACS Appl. Mater. Interfaces* **2011**, *3*, 3205–3214.

14 L. Zhang, D. Taguchi, T. Manaka, M. Iwamoto, *Appl. Phys. Lett.* **2011**, *99*, 083301.

15 F. S. Kim, X. Guo, M. D. Watson, S. A. Jenekhe, *Adv. Mater.* **2010**, *22*, 478–482.

16 A. Babel, Y. Zhu, K.-F. Cheng, W.-C. Chen, S. A. Jenekhe, *Adv. Funct. Mater.* **2007**, *17*, 2542–2549.

17 F. S. Kim, E. Ahmed, S. Subramaniyan, S. A. Jenekhe, *ACS Appl. Mater. Interfaces* **2010**, *2*, 2974–2977.

18 T. B. Singh, S. Günes, N. Marjanoviæ, N. S. Sariciftci, R. Menon, *J. Appl. Phys.* **2005**, *97*, 114508.

19 M. Shahid, T. McCarthy-Ward, J. Labram, S. Rossbauer, E. B. Domingo, S. E. Watkins, N. Stingelin, T. D. Anthopoulosb, M. Heeney, *Chem. Sci.* **2012**, *3*, 181–185.

20 D. Hu, G. Cheng, P. Lu, H. Liu, F. Shen, F. Li, Y. Lv, W. Dong, Y. Ma, *Macromol. Rapid Commun.* **2011**, *32*, 1467–1471.

21 B. Pal, W.-C. Yen, J.-S. Yang, W.-F. Su, *Macromolecules* **2007**, *40*, 8189–8194.

22 Y.-J. Cheng, S.-H. Yang, C.-S. Hsu, *Chem. Rev.* **2009**, *109*, 5868–5923.

23 S. Cho, J. Lee, M. Tong, J. H. Seo, C. Yang, *Adv. Funct. Mater.* **2011**, *21*, 1910–1916.

24 A. J. Kronemeijer, E. Gili, M. Shahid, J. Rivnay, A. Salleo, M. Heeney, H. Sirringhaus, *Adv. Mater.* **2012**, *24*, 1558–1565.

25 J. C. Bijleveld, R. A. M. Verstrijden, M. M. Wienk, R. A. J. Janssen, *J. Mater. Chem.* **2011**, *21*, 9224–9231.

26 J. H. Kim, J. W. Chung, Y. Jung, S.-J. Yoon, B.-K. An, H. S. Huh, S. W. Lee, S. Y. Park, *J. Mater. Chem.* **2010**, *20*, 10103–10106.

27 X. Zhan, Y. Liu, X. Wu, S. Wang, D. Zhu, *Macromolecules* **2002**, *35*, 2529–2537.

28 H.-C. Yeh, S.-J. Yeh, C.-T. Chen, *Chem. Commun.* **2003**, 2632–2633.

29 Y. Lin, M. E. El-Khouly, Y. Chen, M. Supur, L. Gu, Y. Li, S. Fukuzumi, *Chem. Eur. J.* **2009**, *15*, 10818–10824.

30 L. Huoa, Z. Tan, X. Wang, M. Hana, Y. Li, *Synth. Met.* **2007**, *157*, 690–695.

31 T. Lee, C. A. Landis, B. M. Dhar, B. J. Jung, J. Sun, A. Sarjeant, H.-J. Lee, H. E. Katz, *J. Am. Chem. Soc.* **2009**, *131*, 1692–1705.

32 J. H. Kim, A. Watanabe, J. W. Chung, Y. Jung, B.-K. An, H. Tada, S. Y. Park, *J. Mater. Chem.* **2010**, *20*, 1062–1064.

33 H. Padhy, D. Sahu, D. Patra, M. K. Pola, J.-H. Huang, C.-W. Chu, K.-H. Wei, H.-C. Lin, *J. Polym. Sci. Part A: Polym. Chem.* **2011**, *49*, 3417–3425.

34 J. A. Mikroyannidis, M. M. Stylianakis, P. Balraju, P. Suresh, G. D. Sharma, *ACS Appl. Mater. Interfaces* **2009**, *1*, 1711–1718.

35 B. Lim, K.-J. Baeg, H.-G. Jeong, J. Jo, H. Kim, J.-W. Park, Y.-Y. Noh, D. Vak, J.-H. Park, J.-W. Park, D.-Y. Kim, *Adv. Mater.* **2009**, *21*, 2808–2814.

36 I. McCulloch, M. Heeney, C. Bailey, K. Genevicius, I. Macdonald, M. Shkunov, D. Sparrowe, S. Tierney, R. Wagner, W. Zhang, M. L. Chabinyc, R. J. Kline, M. D. McGehee, M. F. Toney, *Nat. Mater.* **2006**, *5*, 328–333.

37 H.-C. Yeh, W.-C.; Wu, Y.-S. Wen, D.-C. Dai, J.-K. Wang, C.-T. Chen, *J. Org. Chem.* **2004**, *69*, 6455–6462.

38 J. Pomrnerehne, H. Vestweber, W. Guss, R. F. Mahrt, H. Bässler, M. Porsch, J. Daub, *Adv. Mater.* **1995**, *7*, 551–554.

39 G. Klaerner, R. D. Miller, *Macromolecules* **1998**, *31*, 2007–2009.

40 Gaussian 03, revision C.02; Gaussian, Inc.: Wallingford, CT, **2004**.

41 Jaguar, version 6.5; Schrodinger, LLC: New York, 2005.

42 J. Ku, Y. Lansac, Y. H. Jang, *J. Phys. Chem. C* **2011**, *115*, 21508.

43 H.-G. Jeong, B. Lim, S.-I. Na, K.-J. Baeg, J. Kim, J.-M. Yun, D.-Y. Kim, *Macromol. Chem. Phys.* **2011**, *212*, 2308–2318.

44 S. B. Darling, *J. Phys. Chem. B* **2008**, *112*, 8891–8895.

45 J. Liu, I. A. Mikhaylov, J. Zou, I. Osaka, A. E. Masunov, R. D. McCullough, L. Zhai, *Polymer* **2011**, *52*, 2302–2309.

46 Y. Li, F. Li, H. Zhang, Z. Xie, W. Xie, H. Xu, B. Li, F. Shen, L. Ye, M. Hanif, D. Ma, Y. Ma, *Chem. Commun.* **2007**, 231–233.

47 J. Liu, Y. Sun, X. Gao, R. Xing, L. Zheng, S. Wu, Y. Geng, Y. Han, *Langmuir* **2011**, *27*, 4212–4219.

48 M. Surin, E. Hennebicq, C. Ego, D. Marsitzky, A. C. Grimsdale, K. Müllen, J.-L. Brédas, R. Lazzaroni, P. Leclère, *Chem. Mater.* **2004**, *16*, 994–1001.

49 Lee, H. Kong, S.-Y. Oh, H.-K. Shim, I.-N. Kang, J. *Polym. Sci. Part A: Polym. Chem.* **2009**, *47*, 111–120.

50 E. J. Meijer, D. M. De Leeuw, S. Setayesh, E. Van Veenendaal, B.-H. Huisman, P. W. M. Blom, J. C. Hummelen, U. Scherf, T. M. Klapwijk, *Nat. Mater.* **2003**, *2*, 678–682.